EUROPEAN ALUMINIUM
CONGRESS | 2009
23-24 November 2009
Maritim Hotel | Düsseldorf

SESSION 2 - JOINING

# Innovative Joining Methods for Lightweight Designs

Author:
Sonja Huber [1]
Michael Marré [2]
Markus Ruhstorfer [1]
Jens Rautenberg 3
Christian Weddeling [2]
Thilo Hammers [4]
Michael Kronthaler [1]
Matthias Merzkirch [4]
Michael F. Zaeh [1]
Erman Tekkaya [2]
Dirk Biermann [3]
Volker Schulze [4]
Andreas Zabel [3]

**For more Information see Appendix**

INNOVATIVE JOINING METHODS FOR LIGHTWEIGHT DESIGNS

# ABSTRACT

This article presents the joining technologies investigated in the Collaborative Research Centre TR10. They are able to join modern aluminium alloys as well as novel aluminium-based reinforced composite materials. Therefore, the joining characteristics of the pure aluminium alloy, being the matrix material for the reinforcing elements, as well as the composite material are under consideration. To assemble composite aluminium profiles, joining processes and strategies have to be developed which take into account the special characteristics of the basic aluminium alloy and the composite material. The joining technologies in focus are Friction Stir Welding (FSW), Bifocal Hybrid Laser Welding (BHLW), joining by hydroforming and joining by electromagnetic expansion. FSW is a solid state joining process, combining friction and deformation heating to obtain defect-free high quality joints. The BHLW system incorporates an Nd:YAG laser and a high power diode laser. Both lasers are combined in one process zone by a dedicated optical head. This arrangement allows for a hot crack-free joining of aluminium alloys which generally are not weldable by fusion welding. To join using forming processes, the necessary forming pressure was applied by a medium (hydroforming) and by a magnetic field (electromagnetic expansion). The feasibility of joining by forming has been shown experimentally both for conventionally extruded and reinforced profiles. To generate high-quality joints by forming the milling of the connecting elements (nodes) and the preparation of contact areas is necessary. The machined contact areas affect the joint characteristics through surface quality, burr formation, dimensional accuracy and influence of the peripheral zone. Metallurgical investigations and characterization of the mechanical properties of all produced joints were accomplished in order to evaluate the individual welding joints and joints produced by forming. In conclusion, the experimental investigations and the influences of the different materials on the joining processes are outlined and discussed.

## 1. INTRODUCTION

The market's increasing demands for lightweight constructions for reduction of fuel consumption in transportation systems, as well as reduced material resources, are becoming increasingly important. These demands are even more critical due to the current discussion of reducing green house gas emissions caused by production processes. In this context, considerate use of energy intensive materials such as aluminium plays a major role. The Transregional Collaborative Research Centre / TR10 "Integration of forming, cutting and joining for the flexible production of lightweight space frame structures", set up by the German Research Foundation (DFG) at the Universities of Dortmund, Karlsruhe and Munich, specifically aim to research small batch production systems for lightweight space frame structures. Research focuses on the ambitious goal of creating the scientific basis for the development of innovative manufacturing processes and design methods for flexible, integrated process chains. In addition to various joining techniques for aluminium and reinforced aluminium profiles, the investigated production techniques include aluminium three-dimensional curved profile extrusion of continuously reinforced profiles, cutting on the fly and five-axis machining.

Industries worldwide are confronted with the need for an increased use of aluminium alloys in various applications. Therefore, the requirements result in the necessity for a multitude of joining and welding innovations. Applications of modern aluminium alloys are not constricted to simple components anymore. In fact, they are used in ever more complex lightweight structures. However, this complexity can only be achieved with higher geometric flexibility in joining methods and presents a major challenge for new approaches in working with lightweight structures. The described work includes the use of different joining technologies, which are adjusted to the joining areas of the connections on the presented demonstrating structure, a BMW C1 motorcycle space frame (Figure 1).

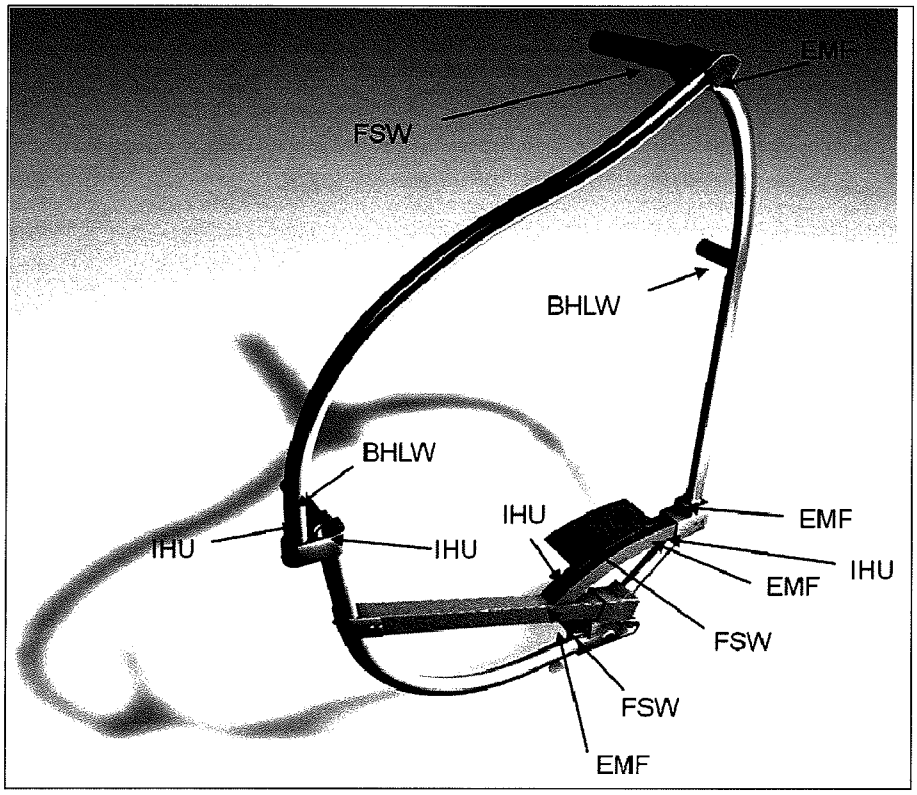


**Figure 1:** Joining areas and the different joining technologies used for the nodes of a BMW C1 motorcycle space frame

The following technologies are employed to assemble the structure:

- Friction Stir Welding (FSW) for joints requiring reinforced profiles
- Bifocal Hybrid Laser Welding (BHLW) for aluminium joints
- Joining by hydroforming (IHU) and electromagnetic expansion (EMF) for reinforced profiles, especially for those closing the final assemblies

## 2. MATERIALS USED IN THE ASSEMBLY

### Materials

The matrix material used in this investigation were the aluminium wrought alloys AA6060 (AlMgSi0.5) and AA6082 (AlSi1MgMn), which is a state of the art material for extrusions in the automotive industry. It is characterized by a good ability to be extruded, as well as good age hardening properties which reduces shape distortion. This reduction in shape distortion makes it possible to produce lightweight structures which are near-net-shape and show adequate strength. The wire material used as a reinforcing element is austenitic spring steel alloy X10CrNi18-8 (1.4310), with a diameter of 1 mm. These materials were chosen by a systematic materials selection study in [1] to provide a list of material combinations suitable for the compound extrusion process and which, additionally, feature good mechanical properties. Investigations were performed using reinforced sheet-metals as well as tubular profiles. The compound extruded reinforced profiles were characterized in [2].

## 3. FRICTION STIR WELDING (FSW)

### Methods and Procedures

Friction Stir Welding (FSW) is a relatively new welding technique which was invented and patented in Cambridge (Great Britain) in 1991 [5]. It is a solid state joining process which combines friction and deformation heating to obtain high quality joints. FSW is a modification of common rotary friction welding, but it does not need the relative movement between the work pieces as joining is achieved by a non-consumable tool. This tool consists of a shoulder and a pin, which are mostly contoured (Figure 2). The tool is forced into the joint partners while undergoing rotational and downward forces, until the shoulder comes into contact with the surface. The friction of the tool shoulder on the surface and the tool pin in the material leads to a local reduction of the material strength due to friction heating. The tool is moved along the joining line as it stirs the heated material. The superimposed movement of both translation and rotation leads to two different weld flanks, the advancing side and the retreating side. When joining is completed, the tool is lifted off of the material.

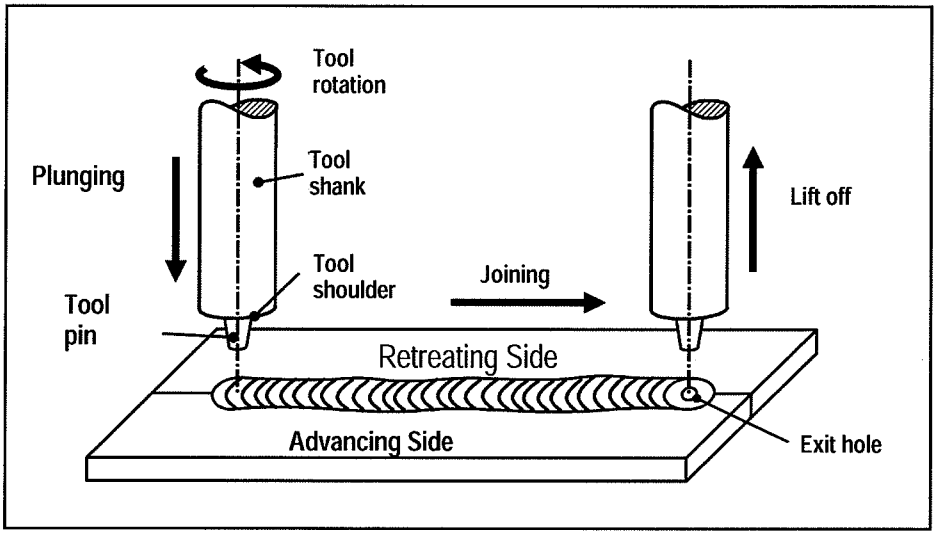


**Figure 2:** Friction Stir Welding process

Figure 3 shows a cross section of the reinforced profiles, which are manufactured at the Institute of Forming Technology and Lightweight Construction (IUL) at the Technische Universitaet Dortmund (Germany). Six steel wires are embedded into the aluminium matrix at a distance of 8 mm apart. The bulk dimensions of the profile are 5 mm x 56 mm. The diameter of a reinforcing element is 1 mm.

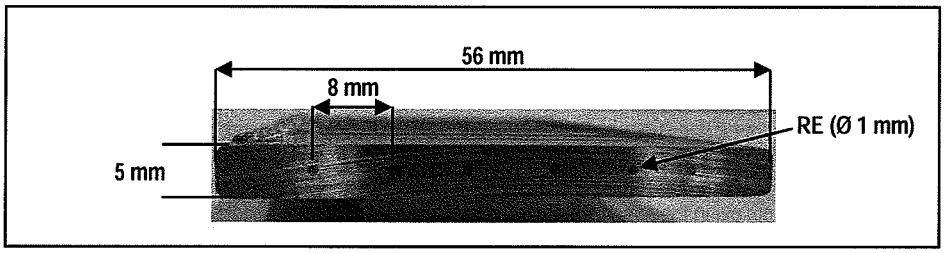


**Figure 3:** Extruded aluminium profile with reinforcing elements

The experiments were conducted on a Heller MCH 250 milling machine with four driven axes. This number of axes allows FSW with a tilt angle, which was set to 2° for all experiments. The Heller MCH 250 is able to weld in position control, like all milling machines, and in force control. Most FSW machines use force control in order to ensure the contact between the tool and the work piece surface. The following experiments were made by position control, because the reinforcing elements lead to significant peaks in the process forces [6]. The reinforced profiles were welded as butt joints. The final destructive testing is a tensile test by using a specimen with two symmetric reinforcing elements in the measurement range.

### Analysis of Joint Characteristics

The absence of a liquid phase during Friction Stir Welding is the reason for the better weldability of the reinforced material. It is possible to join the aluminium matrix material, but not to connect the reinforcing elements. For detailed results it is necessary to analyse the reinforcing elements and in addition their consequences at the welding zone. The method of computed tomography (CT) is a suitable method for this analysis. Figure 4 shows a cross section through the weld joint. Here, different colours symbolize different attenuation of the X-rays. Consequently, this method is feasible to show how the steel reinforcing elements and the base aluminium are distributed. In Figure 4, the reinforcing elements are shown at the centre of the profile. At the advancing side the reinforcing elements are bent upwards towards the surface, which is probably caused by the material flow around the pin because of its threads [7]. A significant amount of steel fragments can be observed in the welding nugget, especially at the advancing side. In order to identify whether the reinforcing elements of the retreating or advancing side caused this accumulation it is necessary to weld samples with only one reinforced joint partner. Metallographic sections of samples with reinforcing elements on the retreating side show that the majority of the steel fragments in Figure 4 originate from this side. Moreover, there is a cavity at the retreating side of the weld nugget.

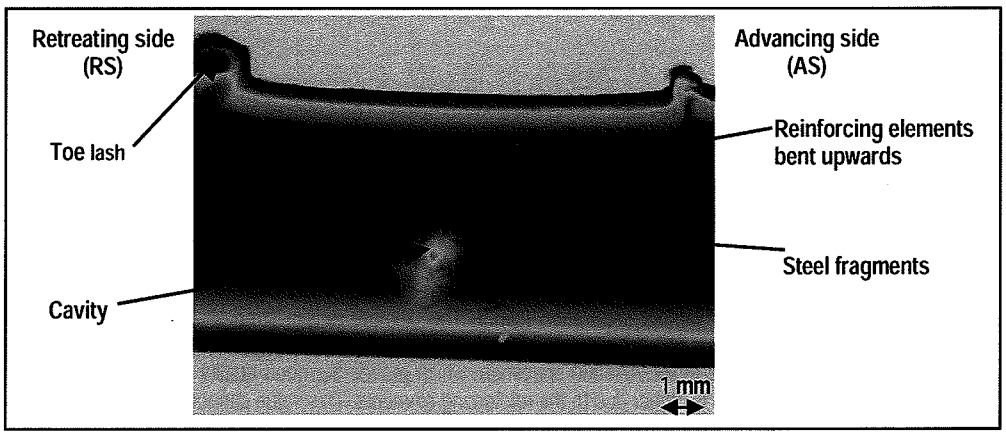


**Figure 4:** µCT photo through an FSW joint (cross section of the weld seam)

A further aspect concerning the behaviour of the reinforcing elements depending on whether their position is on the advancing or retreating side is shown in Figure 5. In this figure a top view of the weld joint can be seen in a computed tomography. The reinforcing elements on the advancing side are not only bent upwards (Figure 4), they are also deformed in the welding direction. At the retreating side, however, most of the steel wires are smashed into small fragments. This behavior is probably caused by the opposing directions of the vectors of welding speed and rotation speed on this side.

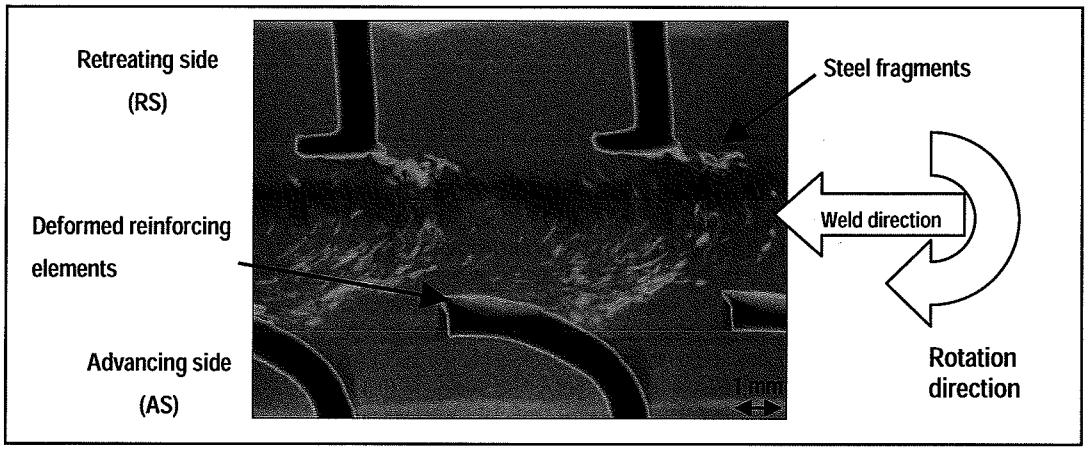


**Figure 5:** µCT photo of the welding zone (top view)

These results show how the reinforcing elements react during the FSW process. The cavities and toe flashes shown in the CT photos can be avoided by optimizing the process parameters and finding a suitable tool configuration. For further experiments a tool with a shoulder diameter of 14 mm and a pin diameter of 5 mm was used. The pin length was 4.7 mm and it was threaded. The shoulder was designed to be flat with concentric grooves. The welding speed was 300 mm/min with a rotational speed of 1500 rpm. The plunge depth was 0.1 mm, which led to a complete weld through the butt joint.

Investigations concerning the pre-treatment before welding with FSW showed no significant influence regardless of whether the specimens were welded after sawing, milling or without separation (blind). The ultimate tensile strength (UTS) of the AA6060 specimens (reinforced and without reinforcements), as well as the ultimate tensile strengths of the specimens welded by FSW, are shown in Figure 6. The strength after welding is comparable to the AA6060 specimen, which proves the good quality of the welding joints. The tensile strength of the reinforced AA6060 specimen is higher due to the reinforcing elements. This value cannot be achieved after welding as the reinforcements cannot be connected by FSW, as shown in Figure 5: µCT photo of the welding zone (top view)

The increased variation after milling and sawing results from the initial gap between the welding partners, which does not exist with blind welding.

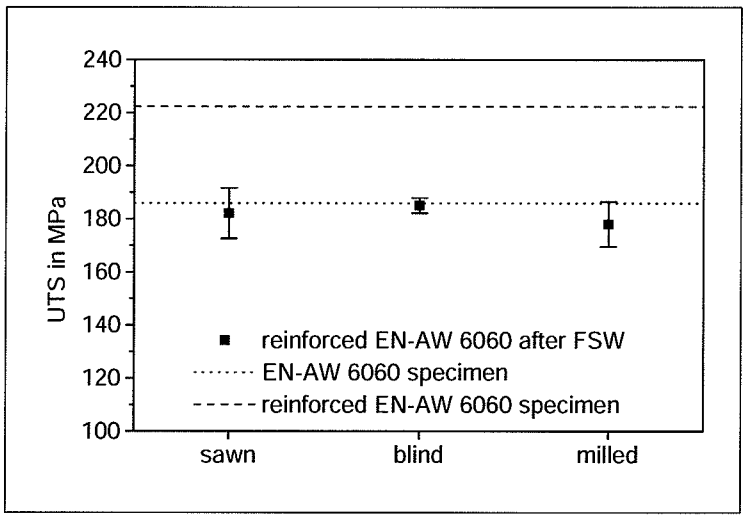


**Figure 6:** Tensile strength of a welded specimen after different pre-treatments before welding compared to an AA6060 specimen with and without reinforcing elements

### Conclusion / Discussion

Friction Stir Welding has the capability to weld steel reinforced aluminium profiles. This joining process joins the aluminium material but not the reinforcing elements. The reinforcing elements are deformed or smashed into small fragments. Although there are steel fragments in the welding zone, the UTS of joint-reinforced specimens are as high as for the non-reinforced, unwelded AA6060 specimens. The process of cutting has no significant influence on the joint's ultimate tensile strength.

## BIFOCAL HYBRID LASER WELDING (BHLW)

### Methods and Procedures

Bifocal Hybrid Laser Welding (BHLW) was investigated and developed at the Institute for Machine Tools and Industrial Management (iwb) at the Technische Universitaet Muenchen. The principle of multi spot laser welding aims at taking beneficial influence on the melt pool geometry during welding. To realize a multi laser spot weld two different techniques are applied: One technique guides the beam of one laser source through an optical system, splitting the beam and creating two autonomous focal spots. This method, called Twin Spot, is well established and showed some favourable advantages for fusion welding [8]. Another technique employs two independent laser sources, which can be of the same or differing types. The experimental set-up for the BHLW incorporates a 3 kW Nd:YAG laser and a 3 kW High Power Diode Laser (HPDL), both integrated by one optical head and acting in the same process zone (Figure 7).

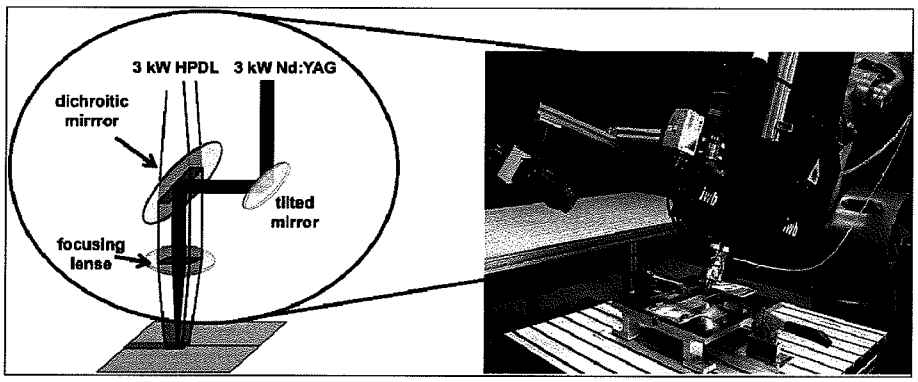


**Figure 7:** experimental set-up for BHLW employs a 3 kW Nd:YAG laser and a 3 kW HPDL

The HPDL is integrated into the optical head and the Nd:YAG laser is linked via a fiber optic cable. A dichroitic mirror carries out the coupling of both laser beams. Its coatings are prepared to be penetrable for the wavelengths of the 3 kW HPDL ($\lambda_1$ = 808 nm, $\lambda_2$ = 940 nm) and fully reflective for the wavelength of the Nd:YAG laser ($\lambda$ = 1064 nm). By adjusting the optical system, the individual positioning of both foci is possible and offers beneficial welding effects. For the discussed results the spot of the Nd:YAG was centred within the rectangular HPDL spot. For fusion welding processes the application of a shielding gas is necessary to prevent oxidization. Therefore the inert argon gas covers the laser process zone with a volume flow rate of $\dot{V}$ = 25 L/h, coaxially with the ray path. For alloys that are difficult to weld a filler wire is necessary. The BHLW system allows filler wire feeding to alloy the weld. The specifications of the whole welding system are defined by the lasers and the optical system. Because the HPDL is transmitted directly with a beam parameter product (BPP) of 85 x 200 mm*mrad, a rectangular focus (f = 150 mm) of 0.9 mm x 3.66 mm can be generated. Unlike the diode laser, the Nd:YAG laser has a BPP of 25 mm*mrad transformed by a focusing lens (f = 150 mm) into a circular focus with a diameter of d = 0.45 mm. Weld seams of an aluminium alloy utilizing the rectangular spot of the 3 kW HPDL are defective and not suitable for even moderate quasi-static tensile loading [9]. Due to the characteristics of aluminium and its alloys for wavelengths of 808 nm and 940 nm and its high thermal conductivity of about 209 W/m*K [10], the intensity of the HPDL is too low to achieve deep penetration. It is consequently not possible to create a characteristic keyhole. Welding of aluminium utilizing the 3 kW HPDL at low welding velocity $v_w = 0.83 * 10^{-3}$ m/s – 0.04 m/s creates a calm melt pool due to heat conduction until melting. It is followed by convectional flow leading to a low aspect ratio [11]. Creating a non-dynamic melt pool during the complete welding process is one of the main advantages of HPDL welding. On the other hand, HPDL welded aluminium joints show only marginal tensile strength. This is caused by entrapments of alumina resulting from the differing phase transition temperatures and densities of aluminium and alumina, which is called a "kissing bond".

Unlike with heat conduction welding accomplished by using a 3 kW HPDL, deep penetration can be achieved using an Nd:YAG laser for aluminium welding. Due to the high energy density within the focal spot of the 3 kW laser, the aluminium vaporizes and generates a keyhole.

BHLW combines the deep penetration effect of an Nd:YAG laser with the benefits of heat conduction welding using the 3 kW HPDL. The beams of the lasers are superimposed in the process zone, thereby inducing several synergetic effects [12]. By virtue of the superposition, the combined welding process differs in energy transfer efficiency compared to the scan of the individual welding processes. This can be partly explained by the calculated absorptivity as a function of temperature for steel and aluminium alloys in the solid and liquid state [10, 13, 14] (Figure 8). The aluminium alloy AA6082 shows approximately 0.6 Vol% more silicon and 0.4 Vol% more manganese than AA6060. This marginal variations allow an estimate of the temperature dependence of the absorption of AA6060. Literature states that the liquidus line of AA6060 is at $T_L$ = 654 °C and the solidus line is at $T_S$ = 616 °C [15]. By means of Figure 8 (II) the increased absorption of the Nd:YAG laser for this temperature range can be assumed to be 8.2% - 10.5%. Since the rectangular HPDL spot is 8 times larger than the spot diameter of the Nd:YAG laser in the y-direction, the 3 kW diode laser heats the welding zone in front of the Nd:YAG laser. At a welding speed of $v_w$ = 0.075 m/s the HPDL is not able to melt the aluminium alloy, but it is heated up close to the melting temperatures (solidus/liquidus temperatures). Spectroscopic temperature measurements showed a temperature of T = 583 °C, which corresponds to an absorptivity increase of 5.8% for λ = 1064 nm. Therefore the HPDL improves the BHLW process by enhancing the absorption of the Nd:YAG laser beam.

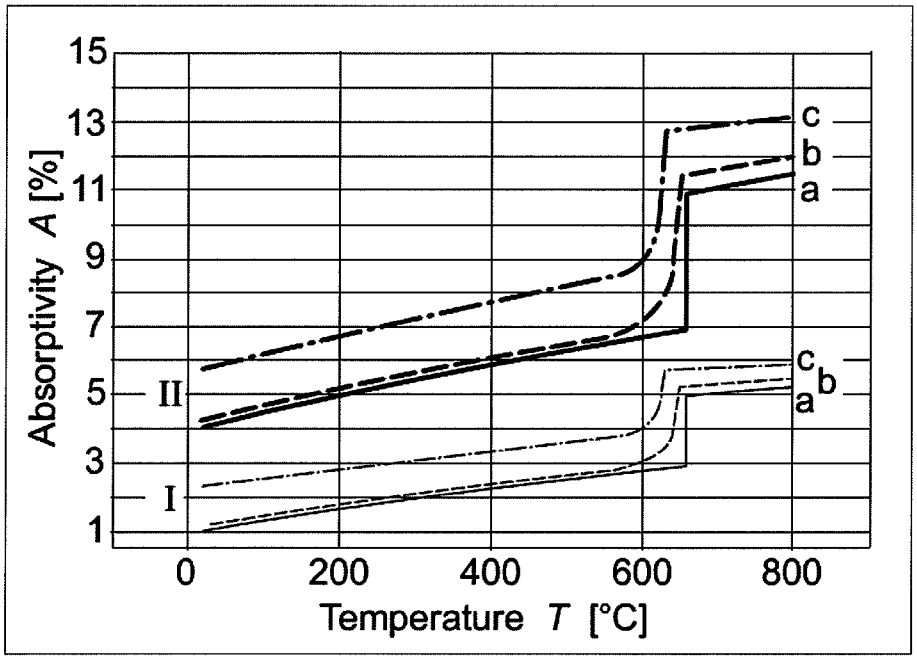


**Figure 8:** Calculated data: Temperature dependence of absorptivity A at (I) 10.6 µm and (II) 1064 nm for (a) Al 99.9, (b) AA6082 and (c) AlMg5 [10]

# INNOVATIVE JOINING METHODS FOR LIGHTWEIGHT DESIGNS

## Analysis of Joint Characteristics

The material used for the manufacturing of joints was the wrought aluminium alloy AA6060. Certain aluminium alloys tend to be susceptible to hot cracks during fusion welding, and the tensile strength of joints may be decreased by hot cracks inside the weld seam. The considered aluminium alloy, in terms of extruded profiles of the AA6060 (AlMgSi0.5) temper state T4, demands the mixture of alloyed filler wire for welding in order to prevent hot cracks. In this investigation the filler wire AlSi12 was used.

During fusion welding of aluminium, hydrogen is the only soluble gas found in an adequate amount in the liquid phase to form pores during solidification [16]. During laser welding, shielding gas is used which can also be responsible for pore formation in deep penetration welding. The shielding gas in combination with some metal vapour can be trapped inside the melt. If it does not leak from the melt before solidification occurs, it will remain as process pores [17]. Two exemplary micrographs of aluminium joints, one with process pores and a second with hydrogen pores, are shown in Figure 9.

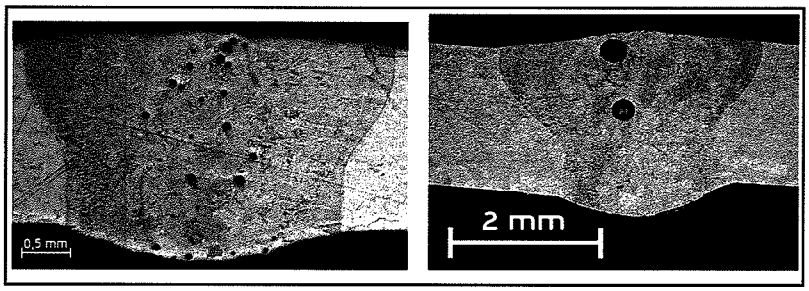


**Figure 9:** Cross sections of aluminium joints with hydrogen pores (left) and process pores (right)

Joints of the aluminium alloy AA6060 welded by BHLW show a significant reduction in porosity. In comparison to the individual Nd:YAG laser, the reduction in porosity is independent of the use of shielding gas [14]. X ray images of the welding process prove the development of process pores at the tip of the keyhole cavity. It is also reasonable, if the time until the melt pool solidifies is too short for the gas bubbles to rise to the surface, that the gas bubbles get entrapped in the melt pool and result in process pores [18]. Since the small Nd:YAG spot is centred in the rectangular HPDL spot, the conducted intensity of the diode laser stabilizes the liquid phase and allows a greater amount of gas bubbles to rise to the surface.

The HPDL also supports a steady solidification of the melt, resulting in a smooth seam surface and a consistent microstructure in its zone of influence (Figure 10). The influence of the HPDL affects the microstructure along the upper 540 µm of the weld seam. There are precipitates at the dendrite rim less than 20 µm in size, whereas the rest of the seam shows precipitations at the dendrite rim larger than 20 µm. This results in a high surface performance with a roughness of $R_t$ = 9.6 µm compared to a pure Nd:YAG weld with a roughness of $R_t$ = 60.3 µm [19].

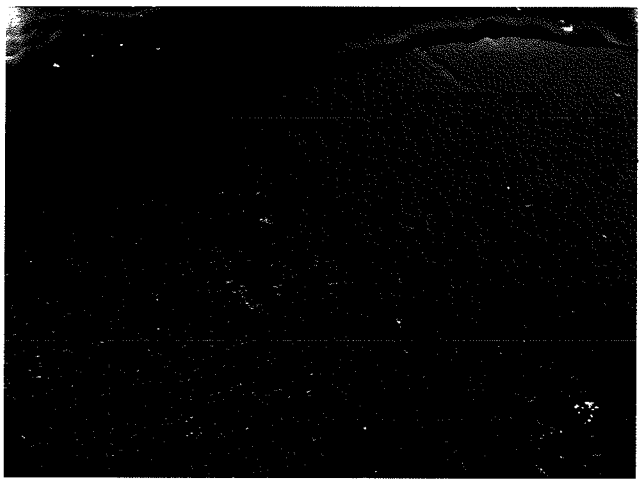

**Figure 10:** Cross section of a seam produced by BHLW with filler wire ($P_{YAG}$ = 3 kW, $P_{HPDL}$ = 3 kW, vw = 0.092 m/s, vd = 0.092 m/s), and examined using scanning electron microscopy

The aim of the presented work is to show the weldability of complex geometries like I-joints and T-joints, which are made up of tubes, to be used as structures in automotive applications. Therefore the laser welded aluminium alloy AA6060 specimens were produced from extruded tubes with an outer diameter of 40 mm and a wall thickness of 2 mm. BHLW I-joints are characterized mechanically and metallographically in order to optimize the hybrid welding process. The welding parameters for the I-joints were chosen as follows: the welding speed was $v_w$ = 0.075 m/s, the filler welding wire material was AlSi12 and the supply feed speed was $v_w$ = 0.075 m/s, which corresponds to the rotation velocity of the tube. The argon flow rate was adjusted to $\dot{u}$ = 25 L/h. For the characterization of selected areas of the weld seam, a flat specimen was cut from welded tubes (tube specimen), with a weld seam located in the middle of the specimen as depicted in Figure 11. To determine characteristic values of maximum achievable ultimate tensile strengths, tensile tests of whole tubes were performed. All tensile tests were conducted quasi-statically using a Zwick 100 kN electromechanical universal testing machine with a traverse velocity of $v_{tra}$ = 1 mm/min.

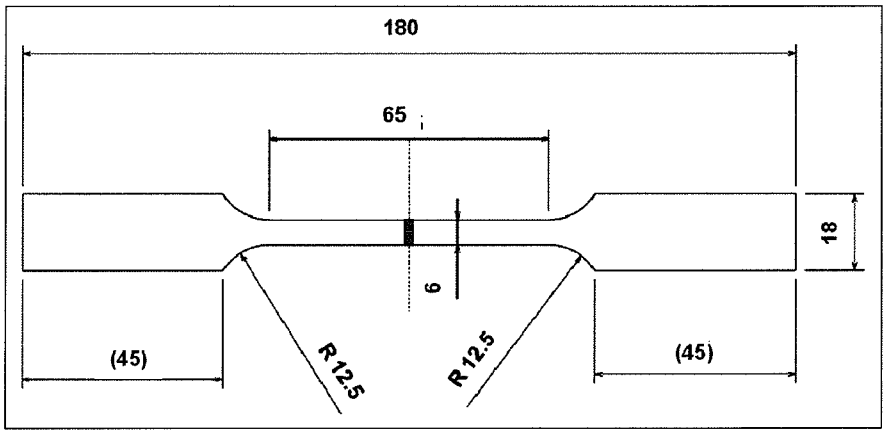


**Figure 11:** Geometry of a tube specimen machined from welded tubes for the tensile tests (weld seam in the middle of the specimen)

For a better mechanical characterization of different areas of the weld seam, several tube specimens of the periphery were taken. Specimens containing the end crater were of particular interest, since the other welding areas are of the same quality as for I-joints of plates. The end crater is the area of the weld seam where the beginning and the end of the weld seam overlap. Due to this re-welding and resulting second heating of the weld seam and the surrounding material, as well as the stopping of the filler wire feed, hot cracks in the weld seam and geometric inaccuracies may occur. In order to analyze the influence of the end crater on the whole I-joint structure the ultimate tensile strength of the whole tube was also determined.

Figure 12 shows the results of the tensile tests of BHLW welded tube I-joints of whole tube and machined tube specimens. The difference in strength of un-welded specimens and tubes is based upon the missing defined measuring gauge and hence the resulting initiation of necking on the tubes. The lower tensile strength of the heat affected zone in welded tube specimens causes a decrease of strength in comparison to untreated specimens. Tube specimens containing an end crater and the welded tubes with end crater show the lowest tensile strengths. A minimization of the end crater is possible by adjusting the laser powers at the beginning of the weld seam overlap. By reduction of the Nd:YAG laser power to $P_{YAG}$ = 500 W a short time before the end of the welding process, the 3 kW HPDL flattens the end crater. The reduction of the Nd:YAG laser power stops the deep penetration and the HPDL keeps the melt as a liquid. The HPDL therefore allows for the almost complete reduction of the end crater, which leads to an increase of the tensile strength by $\Delta\sigma_{UTS}$ = 25 MPa compared to welded tubes without end crater reduction. Consequently the Tube-Tube-I-Joints achieve 89.4% of the tensile strength of the unwelded tubes (Figure 12). This improved welding of the tubes allows an expanded application of tubes in lightweight structures.

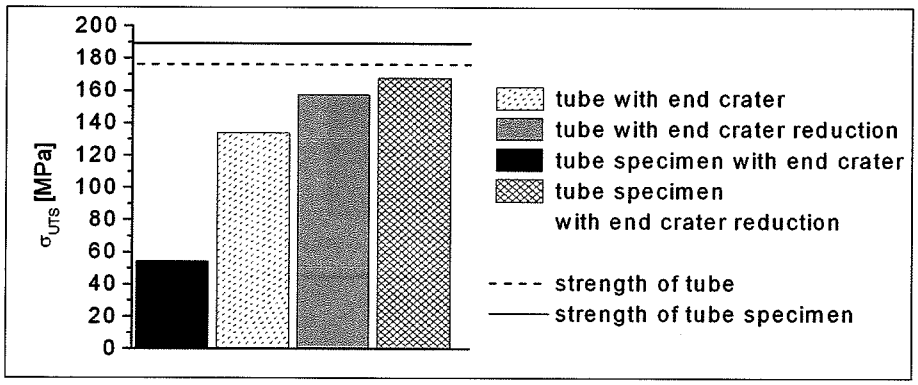


**Figure 12:** Ultimate tensile strengths of tube specimens and whole tubes ($P_{Nd:YAG}$ = 3 kW, $P_{HPDL3}$ = 3 kW, $v_w$ = 0.075 m/s, $v_w$ = 0.075 m/s)

### Conclusion/Discussion

The presented work shows that BHLW of AA6060 is feasible, even for complex structures. HPDLs have various positive effects for welding of aluminium in assisting the Nd:YAG laser during BHLW or deep penetration welding. The metallographic investigations of BHLW Tube-Tube-I-joints showed that the end crater, resulting from the re-welding of the original weld as well as the starting and stopping of the filler wire caused an outer notch effect. This was reduced by the re-welding of the beginning of the weld seam and further supply of filler wire. Consequently, the ultimate tensile strength of whole tubes was increased by about 20 %.

## 5. JOINING BY HYDROFORMING & ELECTROMAGNETIC EXPANSION

### Methods and Procedures

The complexity of the lightweight nodes and their requirements of geometric accuracy and surface quality need precise process planning and adequate machining set-up for manufacturing. Multi-axis machining set-ups provide a high flexibility in development and realisation. They allow milling, drilling, threading and reaming of the nodes from five sides, depending on the machining system being used. The decrease in the number of changes to the clamping set-up avoids interactive defects and geometric inaccuracies and therefore increases the economic efficiency of the process.

From a given CAD model of the frame structure with all the necessary elements, the models of the nodes can be used for further planning (Figure 13). The CAM system, as used for the manufacturing of complex parts like dies and molds, allows the generation of machine specific NC data, depending on which element or surface should be manufactured and which tools and cutting parameters should be used. A Deckel-Maho 5-axis milling and machining centre (DMU 50 Evolution) was chosen to manufacture the lightweight node and its integrated structured surfaces.

There are two basic ways to structure the surface of a joining zone. The micro structure can be described by characteristic surface parameters, e.g. average surface roughness, core roughness depth, or the contact area percentage. This is important for a tight fit between the inner and the outer specimen [20]. Macrostructures can be seen as pockets, grooves and nuts, which allow the profile to fit into or onto the node to obtain a form-fit. The transition between both types of surface characteristics is smooth, with the definition within this article being that macro structures have a visible depth (> 50 µm) and micro structures are only measurable (< 50 µm) but not visible. The micro structured surfaces lead to a more interference-fit-based connection due to the influence of the friction and tangential stresses between both joined elements. Macro-structured surfaces allow a form-fit joint.

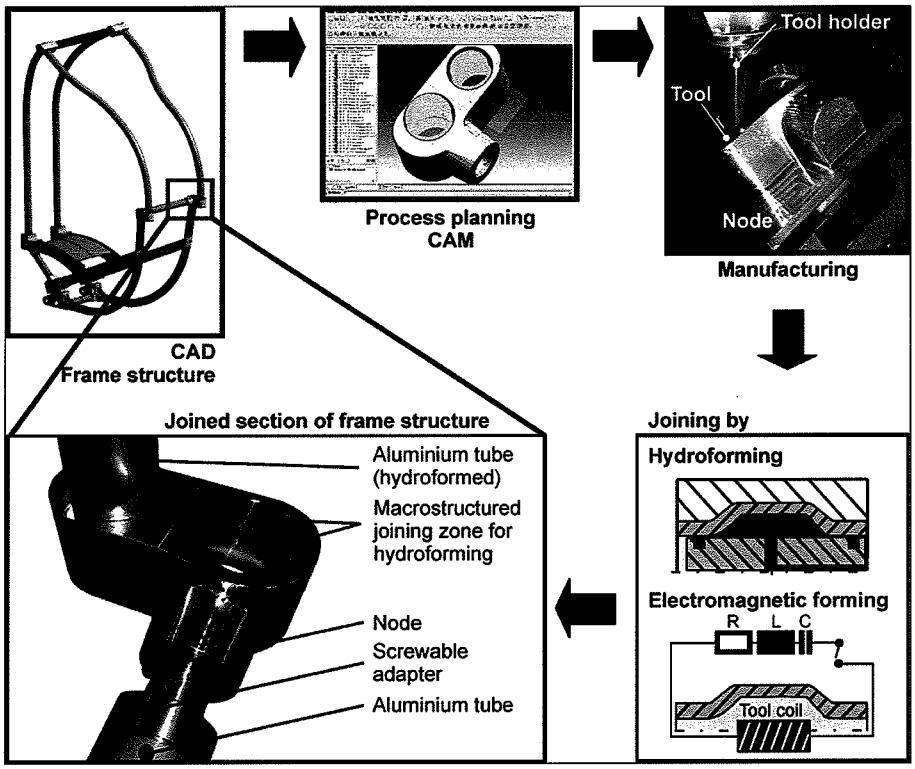


**Figure 13:** Process chain for joining of frame structures

It must be taken into account, however, that the degree of deformation depends on both the material characteristics and the shape (depth, width, length) of the formed element. For the purpose of process-safe, economic, and flexible milling, coated standard ball end mills aluminium were chosen to mill the aluminium. Helical tool paths for the simultaneous five-axis finishing strategies help to keep constant engagement conditions between tool and work piece in order to produce a homogeneous, constant surface quality, to avoid collisions between the tool and the tool holder and to reduce the risk of long, oscillating tools [Wei05]. After production has taken place, one of the forming processes can be used to assemble the frame components (Figure 13).

### Dieless Hydroforming

The process of joining by dieless hydroforming can be divided into three characteristic phases, which are indicated in Figure 14. In the first phase, the tube will be expanded to some value within the clearance (gap $a_0$) limit. After that, both parts (tube and hub) are expanded together until a maximal radial displacement is reached, which is determined by a related joining pressure (Figure 14). The pressure ideally creates elastic and plastic deformation in the tube but solely elastic deformation in the hub. Consequently, Kollmann [21] suggests that for the manufacturing of shrinkage fits a maximum plastic deformation of approximately 30% should be attained, relative to the total cross section of the joining partner. After releasing the pressure, both tube and hub recover elastically. Subsequently, the elastic recovery of the hub is prevented due to the plastic deformation remaining in the expanded tube (Figure 14).

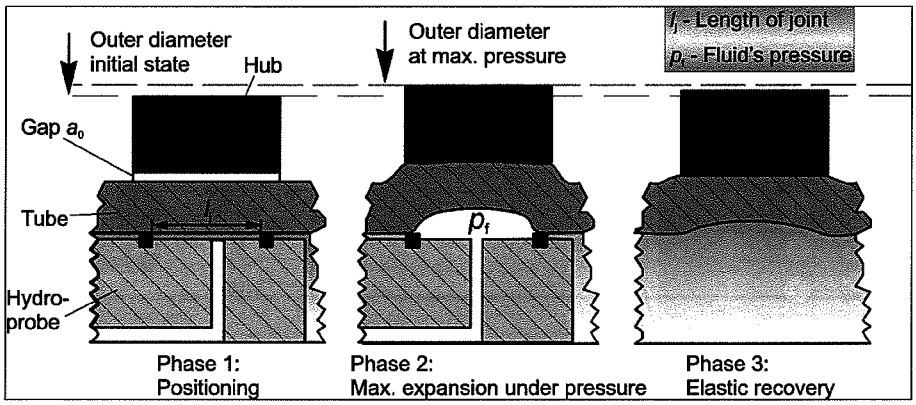


**Figure 14:** Process chain for joining of frame structures

Furthermore, the prevented elastic recovery of the hub results in an interference fit between the joining partners (tube and hub). It is known from the manufacturing of camshafts that if both joint partners possess the same Young's modulus then the joining partners should be arranged with increasing yield points from the inner to the outer joining partner [22]. Joining of aluminium and magnesium, as well as the influence of maximum expansion under pressure, wall thickness of the hub, and initial gap on the strength of the joint, have been briefly presented in [23]. More detailed discussions take tools and repeatability into account [24]. From an engineering standpoint, the working parameter of the fluid pressure $p_i$ represents an important value for estimating the resulting strength of the joint. According to research work performed by Garzke [22], the interference pressure $p$, which is the stress in the contact area of the tube and hub, can be calculated using an approximation.

### Electromagnetic Expansion

Electromagnetic forming (EMF) is a non-contact high velocity process using pulsed magnetic fields to deform materials with high electrical conductivity, such as copper and aluminium alloys. Depending on arrangement and geometry of the tool coil and the work piece, EMF can be used for sheet metal forming operations or for compression or expansion of hollow profiles [25]. Figure 15 shows the typical set-up of work piece, tool coil and forming machine for the electromagnetic expansion of a square tube. This set-up can be represented by a resonance circuit in the equivalent circuit diagram. Within this diagram the forming machine is symbolised by the capacitance $C$, the inner resistance $R_i$ and the inner inductance $L_i$. The work piece and the tool coil can be seen as the consumer load. Due to a sudden discharge of electricity from the capacitor, a damped sinusoidal current $I(t)$ runs through the coil. This current, which typically ranges from 10 to 1000 kA, generates a magnetic field $H(r,z,t)$ around the coil within several microseconds. According to Lenz's law, this magnetic field induces eddy currents in the work piece which are in the opposite direction of the coil current, and shield the magnetic field. The energy density of the magnetic field represents a pressure $p(z,t)$ acting orthogonally on the workpiece [25]. Plastic deformation of the tube will occur once the stresses in the work piece due to this pressure exceed the yield stress of the material.

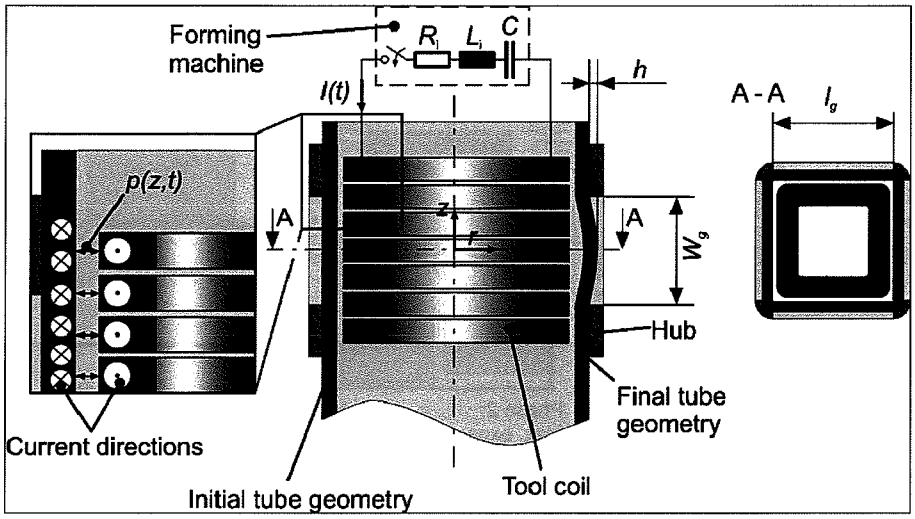


**Figure 15:** Principle of the production of a square tube-to-hub joint by electromagnetic expansion

A currently well investigated application of EMF in research is the forming of sheet metal where the work piece can either be deformed freely or into a die to create a defined shape. The process can also be used to calibrate work pieces which were pre-formed by a conventional quasi-static process [26] or for cutting/shearing operations, but the most commonly used industrial application of EMF is the joining of closed hollow profiles. By using electromagnetic compression or expansion it is possible to produce dominating interference-fit joints or dominating form-fit joints [27]. In the case of very high impact velocities of the electromagnetically driven part it is possible to produce adhesive bonds between the joining partners. This application is called magnetic pulse welding [28]. The strength of the interference-fit depends on the area of the contact zone, the friction coefficient and the residual interference stresses in the contact zone. The interference stresses are influenced by the material properties of the joining partners, such as yield stress and Young's modulus. The geometrical stiffness of the part to be joined also affects the interference stresses [29]. According to [30] and [31] the strength of interference-fit joint produced by electromagnetic compression depends on the geometry and the shape of the groove as well as on the number of grooves. Both authors used cylindrical specimens for their analyses.

### Analysis of Joint Characteristics

#### Strength of hydroformed joints

The strength of the joint against an axial load is mostlydependent on the area of contact $A_{con}$, the interference pressure $p$, and the friction coefficient $\mu$ between the two joining partners, as indicated in equation (1)

$$F_{ax} = A_{con} \cdot \mu \cdot p \tag{1}$$

The area of contact $A_{con}$ depends on the length of the joint $l$ as well as the interference diameter, and is directly proportional to the resulting axial load $F_{ax}$. However, the interference pressure depends on the inner and outer diameter of joining partners, material characteristics as yield stress, Young's modulus, and Poisson's ratio, and the maximum fluid pressure during joining. Joining of two tubes made from the same material results in a low maximum axial load [27]. As a result, for an appropriate axial load to be achieved, a modification of the coefficient of friction seems reasonable. Therefore, adequate manufacturing strategies, developed by the ISF, to specifically adjust the roughness of the tube have been applied and its results on the strength of the joint have been investigated. In addition to the surface finishing by machining, burnishing was also applied as a forming process for surface finishing. The mean roughnesses achieved by the mentioned processes were $R_a$ = 0,63 µm by burnishing, $R_a$ = 3,4 µm to $R_a$ = 7,5 µm by milling [32] and $R_a$ = 10 µm by turning. To generate a disproportionately high roughness a knurl pattern was applied to the surface by a milling process, so that a calculated roughness of $R_a$ = 250 µm was found. Tubes prepared so far were made from aluminium AA6060, with an outer diameter of 40 mm and a wall thickness of 2 mm. They were joined with ring-shaped hubs that had an outer diameter of 50 mm and a wall thickness of 5 mm. Taking the results of preliminary investigations [33] into account an acceptable tangential strain of approximately 1.5 % was detected, and the gap $a_0$ was set to 0 mm. The pressure in phase 2 was adjusted to 74 MPa, resulting in an expansion of 0.4 mm. After joining, an axial load

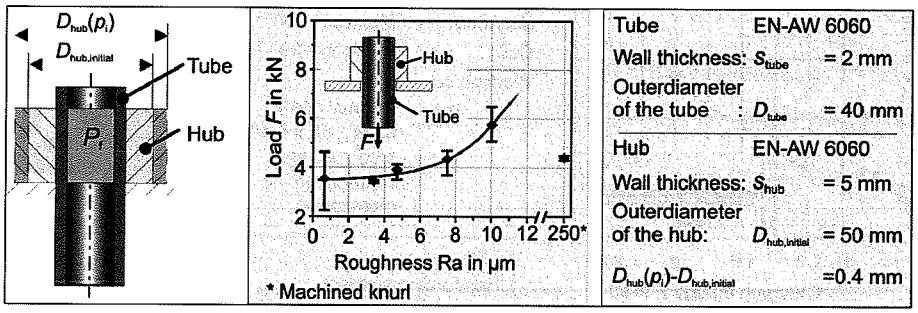


**Figure 16:** Axial load depending on the surface finish of joints made by dieless hydroforming

At first, an increase of the average surface roughness led to an increase of the axial load. Tubes with a knurled surface were significantly less resistant to deformation during tensile tests compared to specimens with a milled surface. As a result, the peaks created by knurling the tube surface were too large to generate an appropriate undercut with the opposite surface of the hub. Moreover, a penetration of the roughness peaks into the opposite surface did not occur as the pressure had already led to the maximum expansion. Using a die, an increase of fluid pressure could lead to the mentioned penetration. Consequently, as only the tips of knurling were in contact to the inner surface of the hub, the area of contact was significantly smaller compared to the machined specimens. Since the area of contact is directly proportional to the axial load, the reduction in maximum axial load is clearly evident.

### Joining of square reinforced aluminium profiles by electromagnetic expansion

Previous analysis regarding the strength of form-fit joints considered primarily tubular specimens deformed by electromagnetic compression [30], [31]. This work is a first experimental approach to extend these analyses of form-fit joints towards reinforced square tubes produced by electromagnetic expansion. To generate the form-fit joints a specified area of the tube was expanded into the grooves of the outer joining partner, the hub (see Figure 15). The square tool coil used within these experiments has an edge length of 40 mm and a length of 30 mm with 8 turns (E-40sqr-8/30). For this first approach the groove width $w_g$ and the groove length $l_g$ (see Figure 15) were kept constant. For $w_g$ a value of 20 mm was chosen, which equals four times the wall thickness of the profiles. For the magnitude of $l_g$ the inner diameter of the tubes was chosen (40 mm). The height of the buckles $h$ was varied by changing the acting magnetic pressure and the charging energy $E$ of the capacitor bank. The maximum height of the buckles was restricted by the beginning of debonding at the interface between the reinforcement wire and aluminium matrix. During the expansion of the tube the reinforcement wires are elongated. Due to volume constancy an increasing elongation leads to a decrease of the cross section and, therefore, to a separation of matrix material and wires [29]. Debonding at the interface disables or reduces load transmission between matrix and wire, and therefore is not acceptable. To determine the maximum allowable deformation and the corresponding charging energy for the joining, a preliminary test series was performed whereby the profiles were expanded with different charging energies within a defined area and restricted by solid collars. The distance between collars was equivalent to the groove width $w_g$. The set-up of the preliminary experiments is shown in Figure 17. After the deformation the heights of the resulting buckles were measured with a coordinate-measuring machine. The results show that an increase in charging energy leads to an increase in deformation.

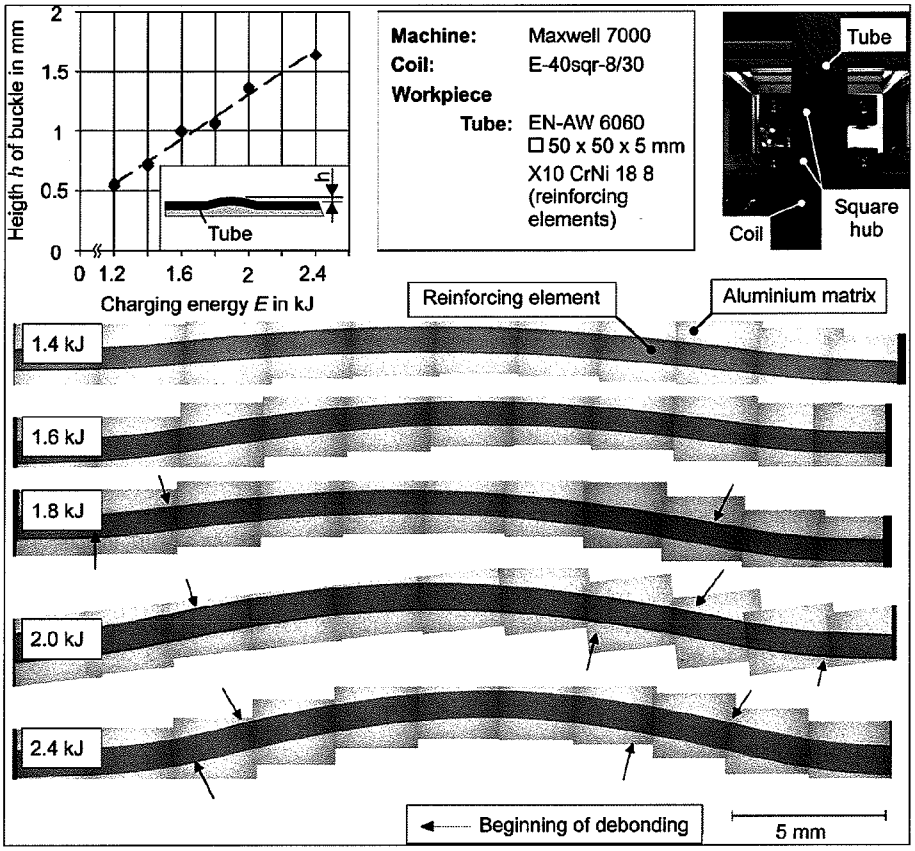


**Figure 17:** Top: Set-up and results of the preliminary tests for the expansion of reinforced square tubes; bottom: Micrographs of the expanded tubes parallel to the wire

In order to evaluate the quality of the bonding between the aluminium matrix and the reinforcement elements, micrographs of the electromagnetically formed specimens were prepared (see Figure 17), which also clearly show the increasing deformation of the tube with increasing charging energy. Charging energies of up to 1.6 kJ did not result in debonding at the interface between the matrix material and the wire. A further increase of the charging energy led to debonding at the interface, marked with arrows in Figure 17. Based on these preliminary tests, a maximum charging energy of 1.8 kJ was chosen for the joining experiments. Although a very little amount of debonding was observed at this energy, it was assumed to have no influence on the material strength. To separate the influence of a pure form-fit from the strength of the joint, all specimens were lubricated with Teflon grease before joining. As a result, the friction coefficient between the joining partners was lowered to a negligible level. Therefore, it was possible to nearly prevent an additional interference-fit in the areas surrounding the grooves. After preparation the specimens were expanded into the grooves of the hub. Charging energies of 1.2 kJ, 1.4 kJ and 1.8 kJ were used. Afterwards, pullout tests of the joints were conducted using a universal tensile testing machine. The experimental results are shown in Figure 18. The diagram of the pullout force $F$ with respect to $E$ indicates that a higher charging energy and the resulting larger height of the buckles lead to a higher strength of the joint. It can also be seen that the strength of the almost pure form-fit is very low compared to the material strength. This can be explained by the small ratio of the tube deformations compared to its wall thickness, due to the debonding restriction.

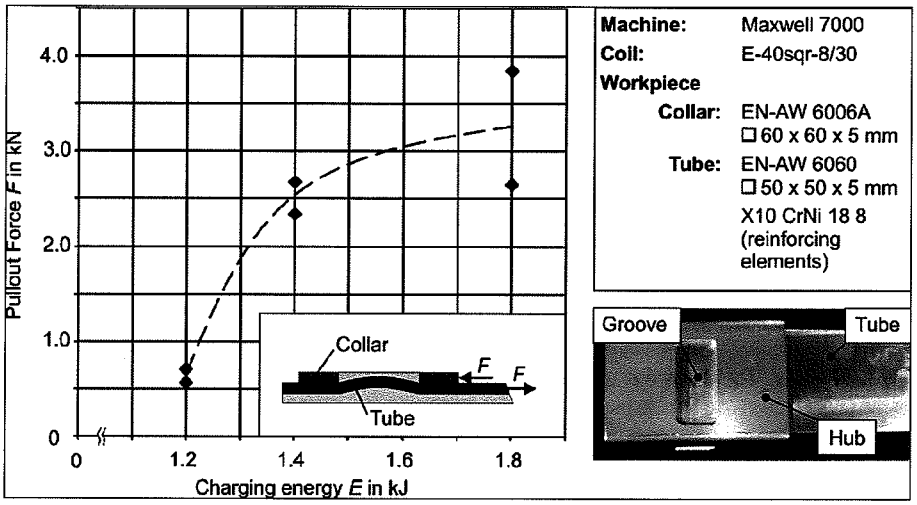


**Figure 18:** Results of the pullout tests of square reinforced tubes joined to square hubs

## Conclusion/Discussion

The necessity of a dedicated structuring of the surface of a joining zone is undeniable. The use of simultaneous five-axis milling strategies allow a reproducible structuring of the surface of lightweight connecting elements in order to control and increase tensile and torsional strength of a joint. Interference-fit joining by expansion of joining partners made from equal material results in a weak interference pressure. As a result, the strength of the joint determined by the area of contact, interference pressure and the coefficient of friction can be increased by modifying the surface structure. Consequently, experimental investigations conducted so far have confirmed the possibility of increasing the strength of the joint by increasing the average surface roughness. However, there is a limit to the increase in strength which can be achieved by increasing the roughness.

The joining experiments of reinforced square aluminium tubes by electromagnetic forming showed that an increase in the height of the buckles leads to an increase in the strength of the joint. It was also shown that the resulting joint strength was low within these tests due to the small allowable deformation. To achieve reasonable strengths of the joints, a combination of an interference-fit and form-fit would be better. Also, an optimisation of the form-fit might be helpful to increase the transferrable load. In the case of non-reinforced tubes it can be assumed that significantly higher joint strengths can be achieved, since larger deformations are feasible. Hence, the knowledge of the interrelation between specific surfaces and the resulting effects on the quality of the joint allows the configuration of a flexible process chain for machining and joining lightweight frame structures.

## 6. CONCLUSIONS

The presented innovative joining methods allow for flexible manufacturing of lightweight frame structures in limited-lot production. They enable an economic production process and lead to a lower structure weight.

Experiments show the weldability of steel reinforced aluminium profiles by using Friction Stir Welding. This method is able to join the aluminium matrix material, but does not connect the reinforcing elements. The pre-treatment (sawing, milling) of the specimen has no significant influence on the joint strength. The aluminium alloy AA6060, which is nearly impossible to fusion weld, can be joined by using Bifocal Hybrid Laser Welding. It could be shown that tube-tube-I-joints can be produced with 93% of the tensile strength of the tubes by using an end crater reduction strategy. For modern joining by forming processes an undeniable necessity for dedicated structuring of the surface of the joining zone exist. The knowledge of the interrelation between specific surfaces and the resulting effects on the quality of the joint allows for the configuration of a flexible process chain for machining and joining lightweight frame structures.

## 7. ACKNOWLEDGEMENT

This paper is based on investigations of the Transregional Collaborative Research Centre SFB/TR10, which is kindly supported by the German Research Foundation (DFG).

## REFERENCES

[ 1] **Weidenmann, K. A.; Fleck, C.; Schulze, V.; Löhe, D.,** Materials selection process for compound-extruded aluminium matrix composites. In: Advanced Engineering Materials, 7 (2005) 12, pp. 1150-1155

[ 2] **Weidenmann, K. A.; Kerscher, E.; Schulze, V.; Löhe, D.,** Mechanical properties of wire-reinforced aluminium extrusions under quasi-static loading conditions. In: Advanced Materials Research: Flexible Manufacture of Lightweight Frame structures, Band 10 (2006), pp. 23-34

[ 3] **Kelly A., Davies G. J.,** The Principles of the Fibre Reinforcement of Metals. Metallurgical Reviews, 10 (37), pp. 1-78, 1965

[ 4] **Courtney T. H.,** Mechanical Behavior of Materials. McGraw-Hill, New York, 1990

[ 5] **Thomas, W. M.:** Patent WO9310935 (27/11/1992). Improvements relating to Friction Welding (06/12/1991)

[ 6] **Ruhstorfer, M.; Zaeh, M. F.:** Friction Stir Welding of Steel reinforced Aluminium Extrusions. In: TWI Ltd. (Ed.): Proceedings of the 7th International Symposium on Friction Stir Welding. Awaji-Island, Japan, 20th - 22nd May 2008

[ 7] **Dubourg, L; Dacheux, P.:** Design and properties of FSW tools: a literature review. In: Proceedings of the 6th International Friction Stir Welding Symposium, Saint-Saveur, Canada, 2006

[ 8] **Schinzel C. M.,** "Nd:YAG Laserstrahlschweißen von Aluminiumwerkstoffen für Anwendungen im Automobilbau," Lasers in Manufacturing 2001, Proceedings of the First International WLT-Conference on Lasers in Manufacturing, 1, Munich, 2001

[ 9] **Trautmann A., and Zaeh M. F.,** "Laser Bifocal Hybrid Welding of Aluminium"; In: Advanced Materials Research: Flexible Manufacture of Lightweight Frame Structures, pp. 65-77 (2006)

[10] **Hügel H., and Dausinger F.,** Fundamentals of laser-induced processes, In: Landolt Börnstein; Springer, Berlin (2004)

[11] **Härtl J.,** Prozessgaseinfluss beim Schweissen mit Hochleistungsdiodenlasern Herbert Utz, München (2006)

[12] **Kleiner M., Baier H., Fleischer J., *et al.,*** Integration von Umformen, Trennen und Fügen für die flexible Fertigung von leichten Tragwerkstrukturen, Ergebnisbericht der Phase I, VDI, Düsseldorf, pp. 153–181 (2003)

[13] **Wieting T. J., Schriempf J. T.,** "Infrared absorptances of partially ordered alloys at elevated temperatures," In: Journal of Applied Physics, 47, 4009 (1976)

[14] **Dausinger F.,** Strahlwerkzeug Laser: Energiekopplung und Prozesseffektivität Teubner, Stuttgart (1995).

[15] **AutomationCreations,** [MatWeb - Material Property Data], Automation Creations, Inc., (2008)

[16] **Ransley C. E., Talbot D. E.,** "Wasserstoff-Porosität in Metallen unter besonderer Berücksichtigung des Aluminiums und seiner Legierungen," In: Zeitschrift Metallkunde 46, (1955)

[17] **Katayama S., Seto N., Mizutani M, *et al.,*** Formation mechanism of porosity in high power YAG laser welding, CRC Press, Dearborn, MI, USA (2000)

[18] **Trautmann A., Roeren S., and Zaeh M. F.,** Novel Insights into porosity formation mechansims in Laser Beam Welding of Aluminium, Laser Institute of America, Temecula, CA, USA, 516 (2008)

[19] **Trautmann A., Roeren S., and Zaeh M. F.,** Welding of Extruded Aluminium Profiles by a Hybrid Bifocal Laser System, Meisenbach Bamberg, Erlangen, Germany (2004)

[20] **Hammers, T.; Marré, M.; Rautenberg, J.; Barreiro, P.; Schulze, V.; Löhe, D.; Brosius, A.; Tekkaya, E.:** Influence of mandrel's surface on the mechanical properties of joints produced by electromagnetic compression. In: ICHSF 2008 – 3rd International Conference on High Speed Forming, 11.3.-12.3.2008, Dortmund, Germany, Proceedings, pp. 245 -256, ISBN 3-9809535-3-X

[21] **Kollmann, F.:** Welle-Nabe-Verbindungen, Gestaltung, Auslegung, Auswahl, Springer Verlag Berlin (1984)

[22] **Garzke, M.:** Auslegung innenhochdruckgefügter Pressverbindungen unter Drehmomentbelastung. Dr-Ing. Thesis. TU Clausthal, VDI Verlag Düsseldorf, 2001

[23] **Homberg, W.; Marré, M.; Beerwald, C.; Kleiner, M.:** Joining by forming of lightweight frame structures, In: Advanced Materials Research: Flexible Manufacture of Lightweight Frame Structures, Band 10 (2006), pp. 89-100

[24] **Przybylski, W.; Wojciechowski, J.; Marré, M.; Kleiner, M.:** Influence of design characteristics and manufacturing process parameters on the strength of tubular aluminium joints produced by hydroforming. In: Archives of Mechanical Technology and Automation, Vol.27 Nr. 1, Polish Academy of Science, 2007, pp. 152-167 ISSN 1233-9709

[25] **Bruno, E. J.:** High Velocity Forming of Metals. Dearborn, Michigan: ASTME, 1968

[26] **Psyk, V.; Beerwald, C.; Henselek, A.; Homberg, W.; Brosius, A.; Kleiner, M.:** Integration of Electromagnetic Calibration into the Deep Drawing Process of an Industrial Demonstrator Part. In: Key Engineering Materials Vol. 344 (2007), pp. 435-442

[27] **Marré, M.; Ruhstorfer, M.; Tekkaya, A. E.; Zaeh; M. F.:** Manufacturing of Lightweight Frame Structures by Innovative Joining by Forming Processes. In: International Journal of Material Forming, 2009 – accepted

[28] **Shribman, V.:** Magnetic Pulse Welding for Dissimilar and Similar Materials. In: ICHSF 2008 – 3rd International Conference on High Speed Forming, 11.3.-12.3.2008, Dortmund, Germany, Proceedings, pp. 245 -256, ISBN 3-9809535-3-X

[29] **Marré, M.; Brosius, A.; Tekkaya, A. E.:** Joining by Compression and Expansion of (Non-) Reinforced Profiles – In: Flexible Manufacture of Lightweight Frame Structures - Phase II: Integration, Weinert, K. et al. (eds.), TTP Trans Tech Publications Ltd, Switzerland, Advanced Materials Research (2008) Vol. 43, ISBN 0-87849-385-9, pp. 57-68

[30] **Golovashchenko, S.:** "Methodology of Design of Pulsed Electromagnetic Joining of Tubes," Proceedings of the TMS Symposium "Innovations in Processing and Manufacturing of Sheet Materials", February 11-15th, 2001, New Orleans, Louisiana, pp. 283-299

[31] **Bühler, H.; v. Finkenstein, Eberhard:** Bemessung von Sickenverbindungen für ein Fügen durch Magnetumformung. In: Werkstatt und Betrieb Vol. 104 (1971), pp. 45-51

[32] **Biermann, D.; Weinert, K.; Zabel, A.; Engbert, T.; Rautenberg, J.:** Machining of Lightweight Frame Components. In: Flexible Manufacture of Lightweight Frame Structures – Phase II: Integration, Weinert, K. et al. (eds.), TTP Trans Tech Publications Ltd, Switzerland, Advanced Materials Research (2008) Vol. 43, ISBN 0-87849-385-9, pp. 37-46

[33] **Hammers, T.; Marré, M.; Rautenberg, J.; Barreiro, P.; Schulze, V.; Biermann, D.; Brosius A.; Tekkaya, A. E.:** Influence of Mandrel's Surface and Material on the Mechanical Properties of Joints Produced by Electromagnetic Compression. steel research int., May Vol. 80 (2009) No. 5, S. 366-375; DOI: 10.2374/SRI08SP151

# INNOVATIVE JOINING METHODS FOR LIGHTWEIGHT DESIGNS

## APPENDIX

[1] **Institut fuer Werkzeugmaschinen und Betriebwissenschaften (iwb)**
Technische Universitaet Muenchen
Boltzmannstraße 15
85748 Garching

[2] **Institut fuer Umformtechnik und Leichtbau (IUL)**
Technische Universitaet Dortmund
Baroper Str. 301
44227 Dortmund

[3] **Institut für Spanende Fertigung (ISF)**
Technische Universitaet Dortmund
Baroper Straße 301
44227 Dortmund

[4] **Institut fuer Werkstoffkunde I (iwk I)**
Universitaet Karlsruhe (TH)
Kaiserstraße 12
76131 Karlsruhe